Supporting Information

for

S K-edge XAS as a Probe of Ligand-Metal Bond Covalency: Metal vs Ligand Oxidation in Cu and Ni Dithiolene Complexes

Ritimukta Sarangi,[†] Serena DeBeer George,[§]* Deanne Jackson Rudd,[†] Robert K. Szilagyi,[†,‖] Xavi Ribas,[⊥] Concepció Rovira,[⊥] Manuel Almeida,[ƒ] Keith O. Hodgson,[†,§]* Britt Hedman,[§]* Edward I. Solomon[†]*

[†]Department of Chemistry, Stanford University, Stanford, CA 94305

[§]Stanford Synchrotron Radiation Laboratory, Stanford Linear Accelerator Center, Stanford University, Stanford, CA 94309

[⊥]Institut de Ciència de Materials de Barcelona, Campus de la Universitat Autònoma de Barcelona, 08193 Bellaterra, Spain

[ƒ]Departamento de Química, Instituto Tecnológico e Nuclear, CFMC-UL, P-2686-953 Sacavém, Portugal

*To whom correspondence should be addressed

Fax: (650) 725-0259, Email: Edward.solomon@stanford.edu; Fax: (612) 625-5780,

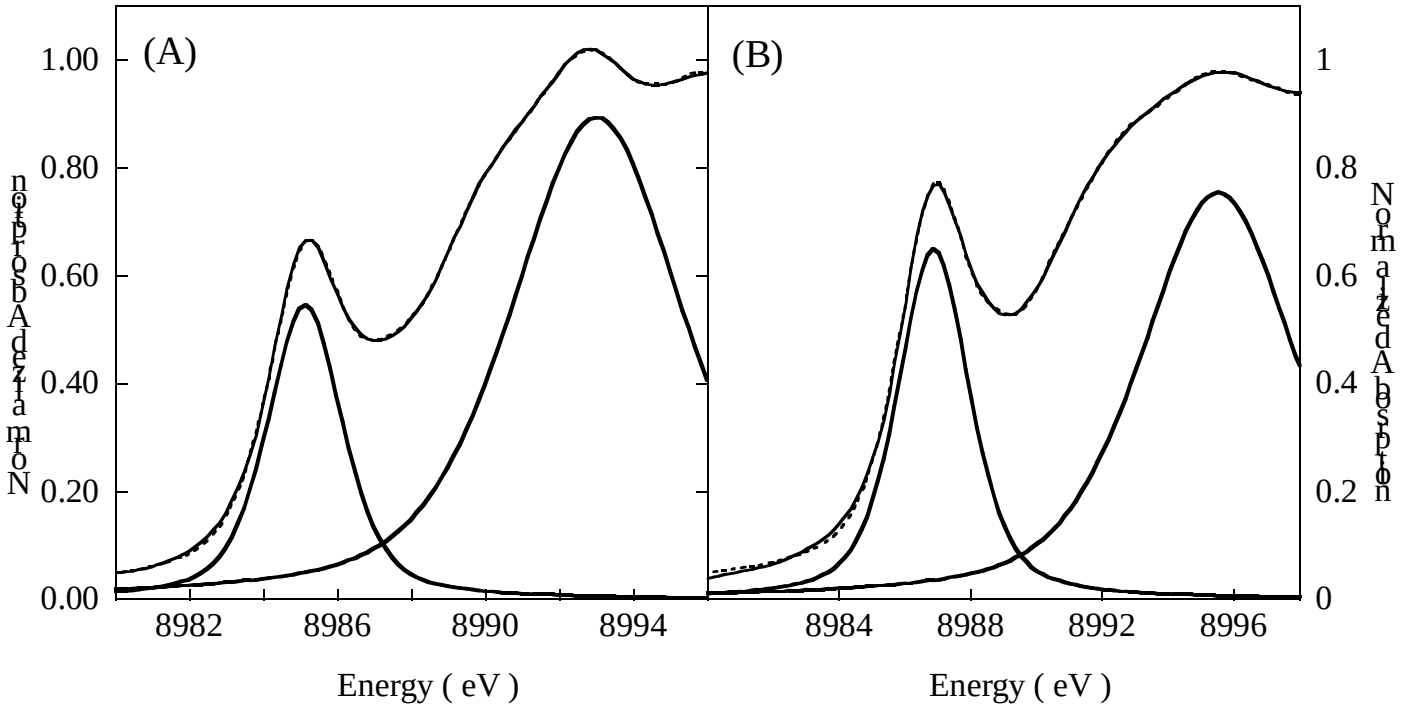

Figure S1. Normalized Cu K-edge X-ray absorption data (—) and fit (- - -). The pseudo-Voigt features used for the 1s → 4p+LMCT shakedown peak (lower energy) and the → 4p transition peak (higher energy) are shown (other peaks are omitted for clarity). **1** (A) and **1ox** (B).

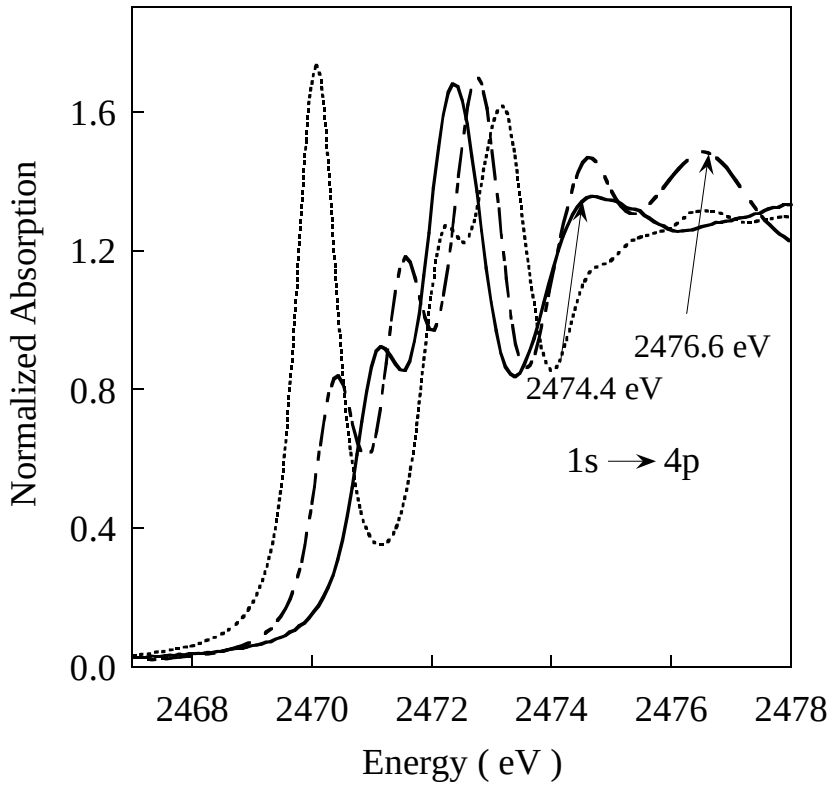

Figure S2. The normalized S K-edge XAS spectra of $(Na)_2$[MNT] (—), **1** (— –) and **1ox** (·····). The lowest energy peak in **1** and **1ox**, which is due to the $1s \rightarrow \psi^*_{\beta-LUMO}$ transition, is absent in $(Na)_2$[MNT].

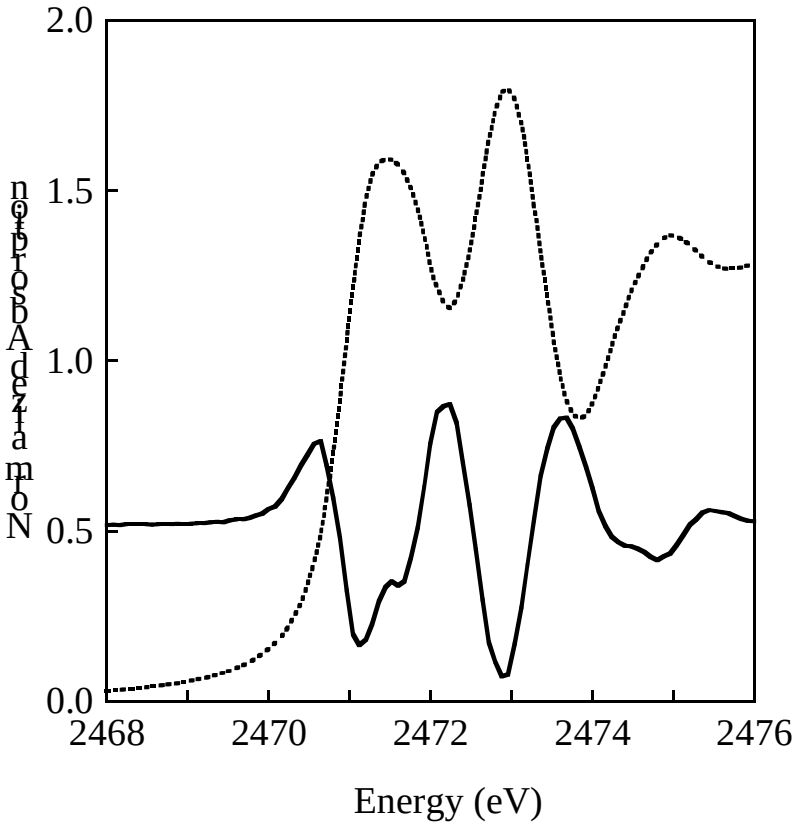

Figure S3. The normalized S K-edge XAS spectra of $(NEt)_2[Ni(MNT)_2]$ (**2**) (**---**) and its second derivative (**—**). The pre-edge and lowest energy edge transitions are clearly resolved in the second derivative spectrum.

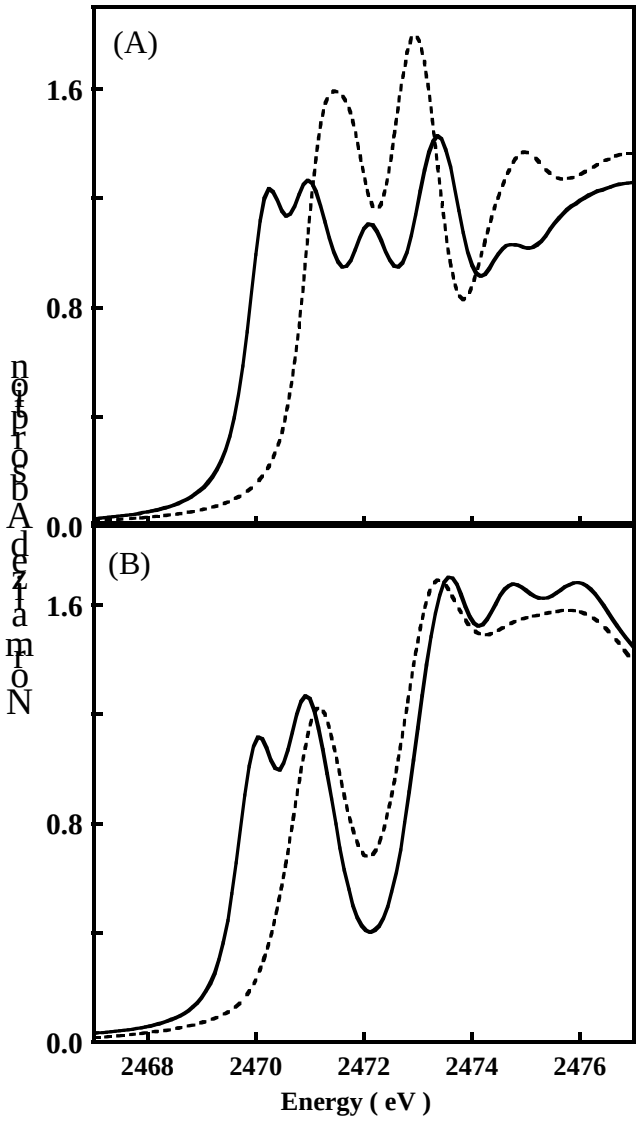

Figure S4. The normalized S K-edge XAS spectra of (A) **2** (**---**) and **2ox** (—) and (B) $[Ni(S_2C_2Me_2)_2]^{2-}$ (**---**) and $[Ni(S_2C_2Me_2)_2]^{-}$ (—). The spectra in (B) have been reproduced from reference 25 (main text). A low energy shoulder in the spectra of $[Ni(S_2C_2Me_2)_2]^{2-}$ which was due to a contamination in the sample, has been subtracted for clarity.

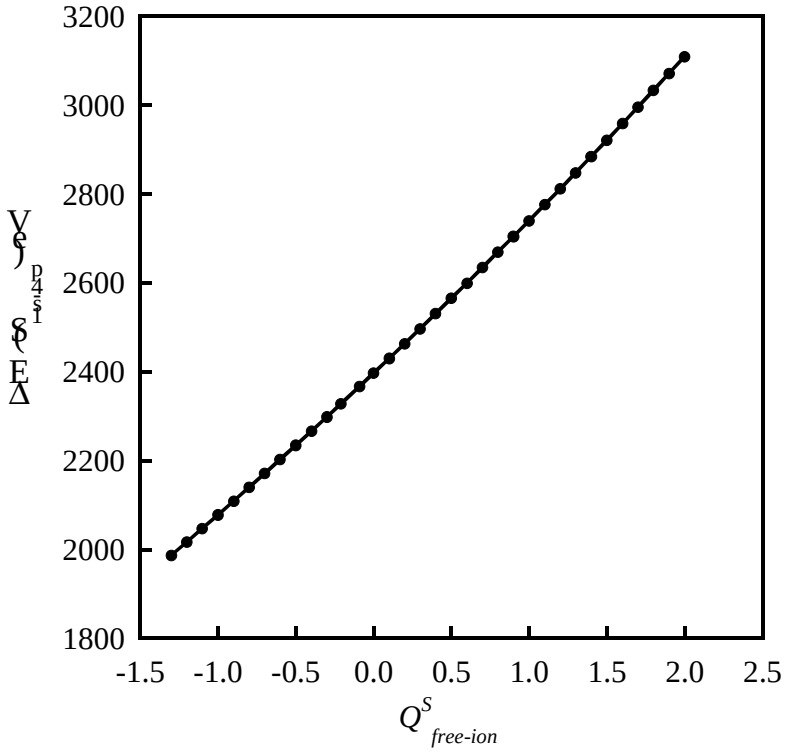

Figure S5. The relationship between change in the charge on the S atom (as a free ion), $Q^S_{free-ion}$, and the calculated energy difference between S (1s) and S (4p) orbital energy [$\Delta E(S_{1s\text{-}4p})$]. The correlation is linear with a ~3% quadratic component.

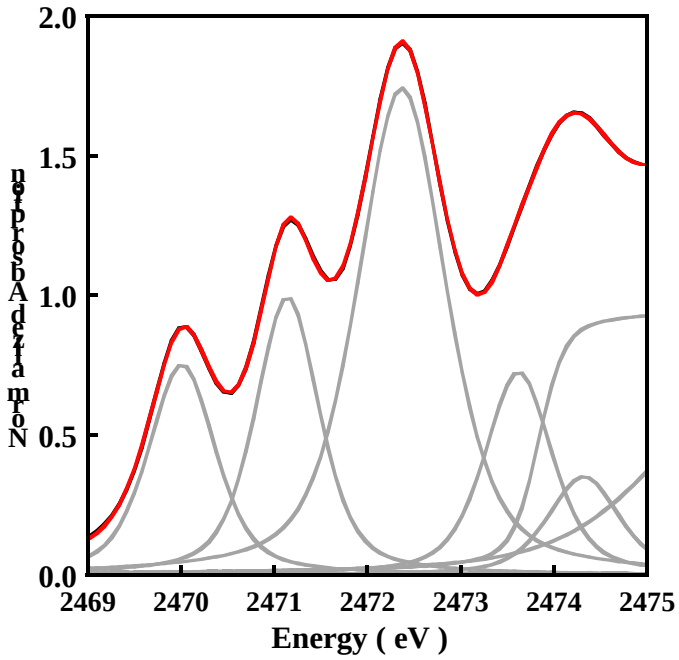

Figure S6. Pseudo-Voigt fits to the S K-edge XAS data of **1**. Data (—), Fit (—) and individual pseudo-Voigt peaks (—)

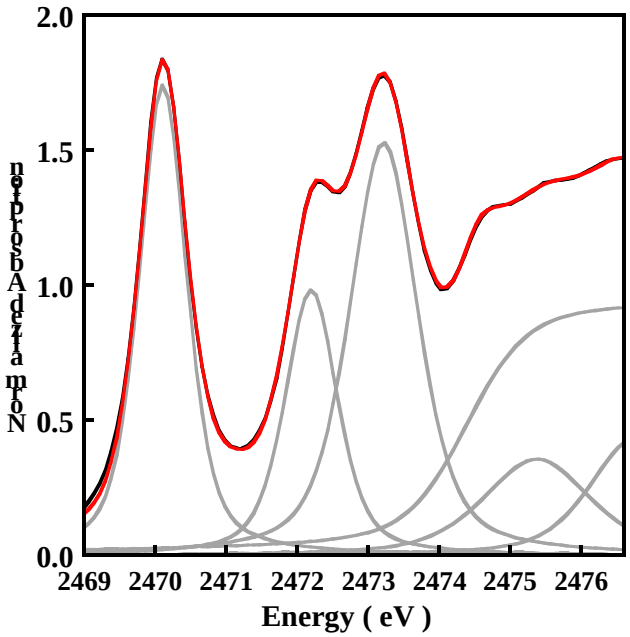

Figure S7. Pseudo-Voigt fits to the S K-edge XAS data of **1ox**. Data (—), Fit (—) and individual pseudo-Voigt peaks (—)

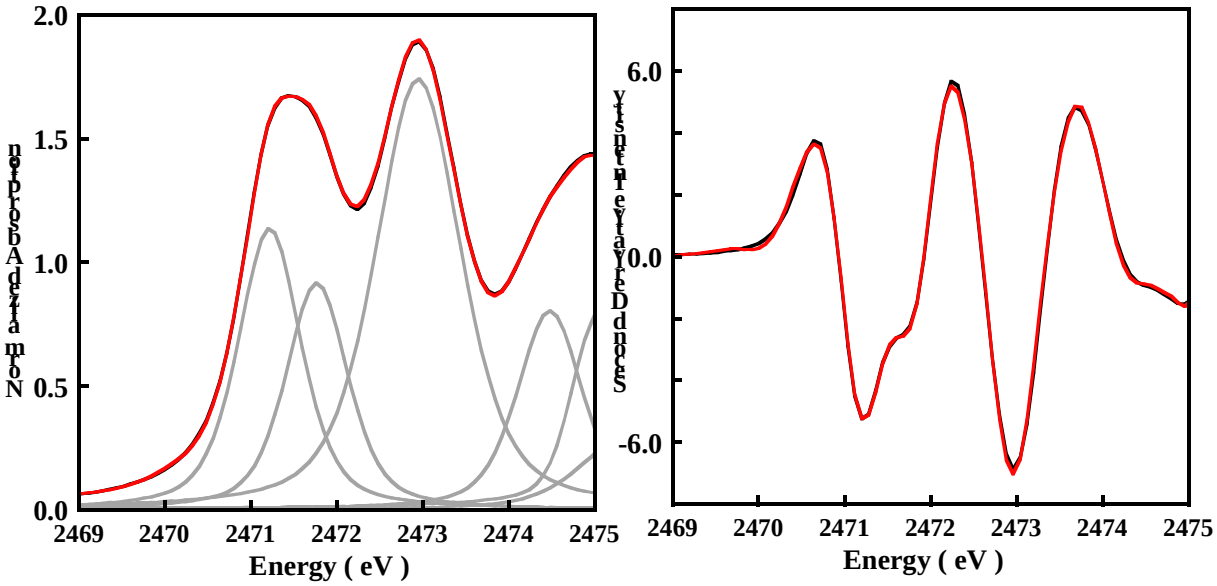

Figure S8. Pseudo-Voigt fits to the S K-edge XAS data of **2**. Data (—), Fit (—) and individual pseudo-Voigt peaks (—). The second derivative data and fit have been shown in the right to demonstrate the goodness of fit between 2470-2472.5 eV.

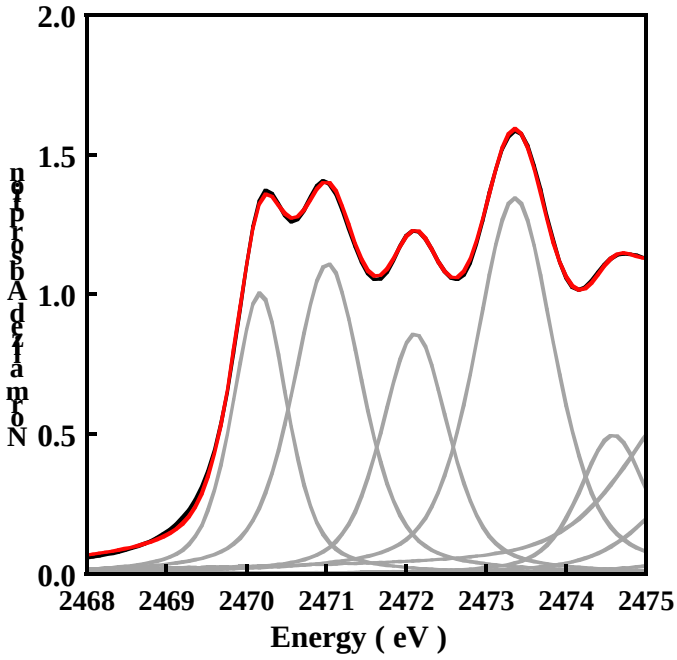

Figure S9. Pseudo-Voigt fits to the S K-edge XAS data of **2ox**. Data (—), Fit (—) and individual pseudo-Voigt peaks (—)

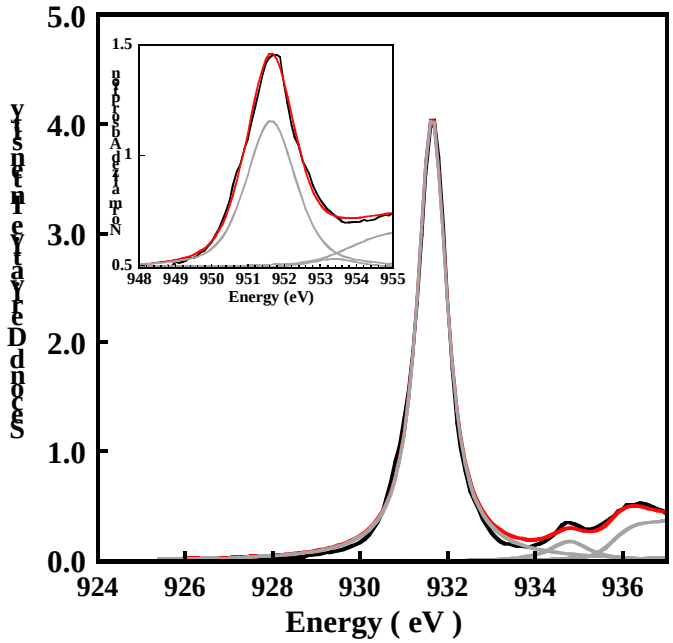

Figure S10. Pseudo-Voigt fits to the Cu L-edge XAS data of **1**. Data (—), Fit (—) and individual pseudo-Voigt peaks (—)

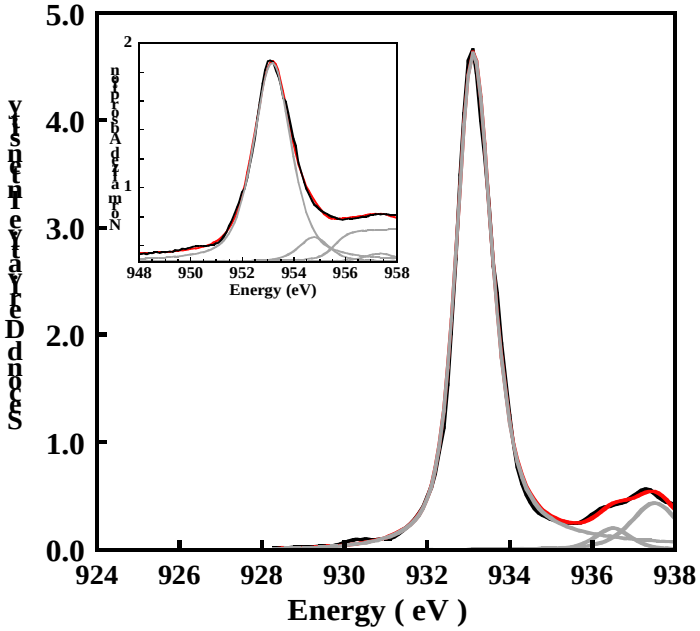

Figure S11. Pseudo-Voigt fits to the Cu L-edge XAS data of **1ox**. Data (—), Fit (—) and individual pseudo-Voigt peaks (—). A <2% Cu(II) contaminant has been subtracted from the spectrum prior to fitting.

S1. Estimation of the 1s→4p transition energy in $[Cu(MNT)]^{2-}$

A combination of S K-edge Data and DFT calculations have been used to estimate the S 1s→4p transition energy in $[Cu(MNT)]^{2-}$. In case of the MNT ligand, both the free ligand $[MNT]^{2-}$ and $[Cu(MNT)_2]^{2-}$ have low lying transitions in their S K-edge data due to low-lying orbitals with S character mixed into the cyano substituents. In order to clearly assign, the S-based transitions and related energy shifts contributing to the S K-edge spectra, a comparison of the S K-edge spectra of $(Na)_2(S_2C_2H_2)$ (**A**) and $(Et_4N)[Ni(S_2C_2Me_2)]$ (**B**) (reported in reference 25) with corresponding DFT calculations has been made first and then the results obtained from this correlation have been applied to the S K-edge data of $(TBA)_2MNT$ and $(TBA)_2[Cu(MNT)_2]$. Figure S12 presents a comparison of **A** and **B**. In the free ligand, two broad transition are observed at ~2472.8 eV and ~2474.2 eV. In **B**, the edge transitions are shifted to higher energy and three transitions are observed at 2473.5 eV, 2474.7 eV and 2475.9 eV. To understand the nature of the orbitals involved in these transitions, DFT calculations were performed on **A** and **B**. The lowest energy valence orbital in both **A** and **B** is the S-C$(\pi)^*$ followed by the S-C$(\sigma)^*$ and S(4p) orbitals. Figure S13(A) shows the DFT calculated energy of the dominantly S based orbitals up to the S 4p with the S-C$((\pi)^*$ aligned at 0 eV for **A** and **B**. The S-C$(\sigma)^*$ orbital in **B** has shifted to higher energy by 1.8 eV relative to the S-C$(\sigma)^*$ in **A**. The S-C bond is shorter by 0.04 A in **B** (1.76 Å) relative to **A** (1.8 Å) which destabilizes the S-C$(\sigma)^*$ orbital in **B** relative to **A**. The 4p orbital is also ~1.4 eV higher in energy in **B** relative to **A** which reflects the increase in Q_{mol}^{S} upon metal binding. This energy spitting is qualitatively consistent with the peaks observed in the experimental spectra of **A** and **B**. Thus, the broad feature at ~2472.8 eV in **A** consists of overlapping S 1s→ S-C$(\pi)^*$and S 1s→ S-C$(\sigma)^*$ transitions which split in energy due to stronger S-C interaction in **B** and occur at 2473.5 eV and

2474.7 eV. The 4p orbital has moved up in energy in **B** to 2475.9 eV relative to 2474.2 eV in **A** reflecting the increase in Q_{mol}^{S} upon Ni binding. The above assignment of the S K-edge spectra of **A** and **B** is next extended to $[MNT]^{2-}$ and **1**. First, a comparison of the S K-edge XAS spectra of $[MNT]^{2-}$ and **A** (shown in Figure S14) is made. In the $[MNT]^{2-}$ spectrum two low-lying transitions are observed: one at 2471.1 eV followed by a broad transition centered at 2472.3 eV. DFT calculation on $[MNT]^{2-}$ indicates the presence of low-lying valence orbitals (with significant S character mixed into the cyano ligands) below the S-C$(\pi)^{*}$ orbital. These orbitals span an energy range of -2.5 eV to -0.4 eV below the S-C$(\pi)^{*}$ orbital, indicating that the 1s→S-C$(\pi)^{*}$ and the 1s→S-C$(\sigma)^{*}$ (which are separated by only ~0.3 eV) overlap with these 1s→S-CN-based transitions and contribute to the higher energy side of the broad peak at 2472.3 eV. Thus, a DFT based assignment of the 1s→S-C$(\pi)^{*}$ is made for $[MNT]^{2-}$ in Figure S14. In addition, by analogy to **A** the S 1s→4p transition is assigned to the next higher energy peak at 2474.6 eV. The S 1s→4p assignment for the free $[MNT]^{2-}$ ligand can now be extended to **1**. A comparison of the S K-edge XAS spectra of $[MNT]^{2-}$ and **1** is shown in Figure S15. Both spectra have low-lying S-CN-based transitions overlapping the 1s→S-C$(\pi)^{*}$ transition (see above). However, the spectrum of **1** shows two transitions to higher energy at ~2474.4 eV and ~2476.6 eV instead of one as observed in $[MNT]^{2-}$ at 2474.6 eV. DFT calculations show that the S-C bond is shorter in **1** (1.77 Å) relative to $[MNT]^{2-}$ (1.80 Å) which destabilizes the S-C$(\sigma)^{*}$ orbital in **1** relative to $[MNT]^{2-}$ (Figure S13). Thus, the peak at 2474.4 eV is assigned to the 1s→S-C$(\sigma)^{*}$ transition which has moved up in energy relative to the free ligand and is now separated from the 1s→S-CN-based and 1s→S-C$(\pi)^{*}$ transitions. Thus, the next transition at 2476.6 eV represents the 1s→4p transition which has shifted to higher energy relative to the $[MNT]^{2-}$ (2474.6 eV) due to increase in Q_{mol}^{S} resulting from binding to Cu which is

in qualitative agreement with the DFT calculations (see Figure S13).

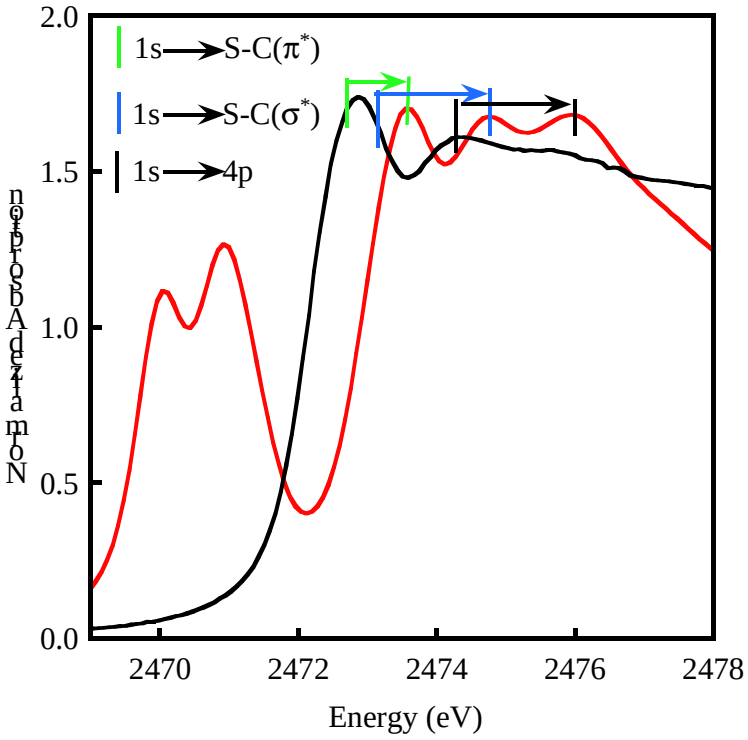

Figure S12. S K-edge XAS spectra of $(Na)_2(S_2C_2H_2)$ (—) and $(Et_4N)[Ni(S_2C_2Me_2)]$ (—). The shift in the 1s→S-C(π)*, 1s→S-C(σ)* and 1s→S(4p) transitions upon Ni binding to the free ligand have been depicted by arrows.

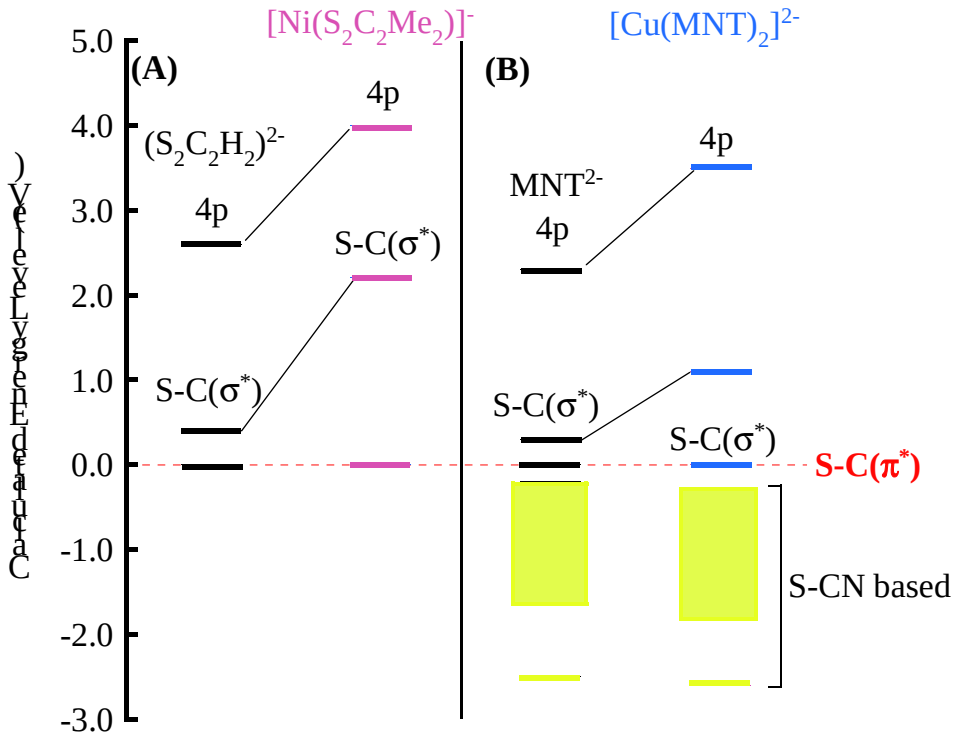

Figure S13. DFT calculated energy levels of the dominantly S-based orbitals (A) **A** and **B** (B) MNT^{2-} and **1**. The S-C(π)* has been aligned at 0 eV for all four complexes. The S-CN-based transitions are shown in light-green in $[MNT]^{2-}$ and **1**.

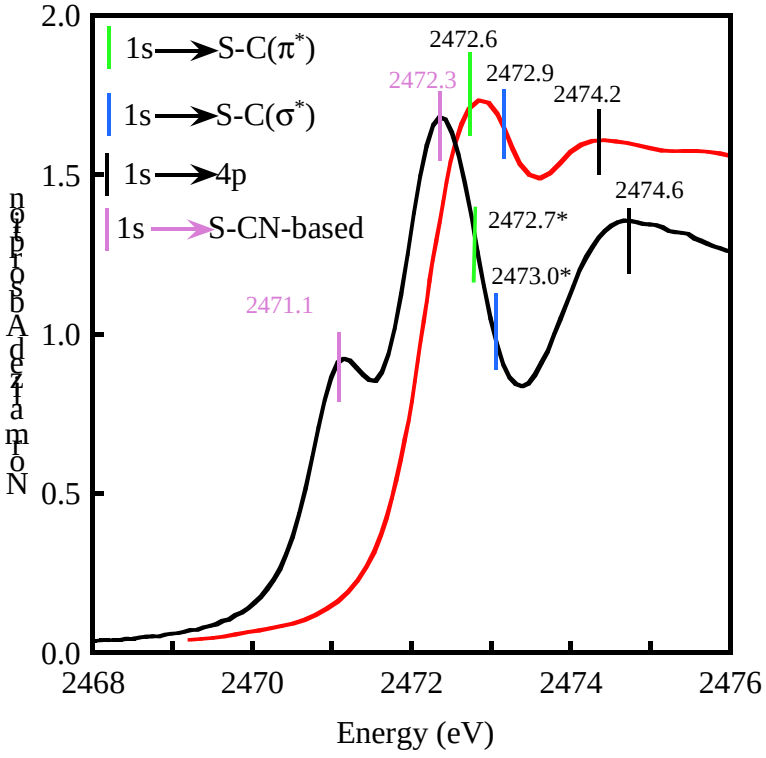

Figure S14. A comparison of the S K-edge XAS spectra of **A** (—) and $[MNT]^{2-}$ (—). The S 1s→ S-C(π)*, S 1s→ S-C(σ)* and S 1s→ 4p transition energies are shown. The low-lying S-CN-based transitions in $[MNT]^{2-}$ are absent in A. The S 1s→ S-C(π)* and S 1s→ S-C(σ)* transitions in $[MNT]^{2-}$ cannot be accurately determined due to overlap with the S-CN based transitions and the values shown here (indicated with a *) are approximate (based on DFT calculations).

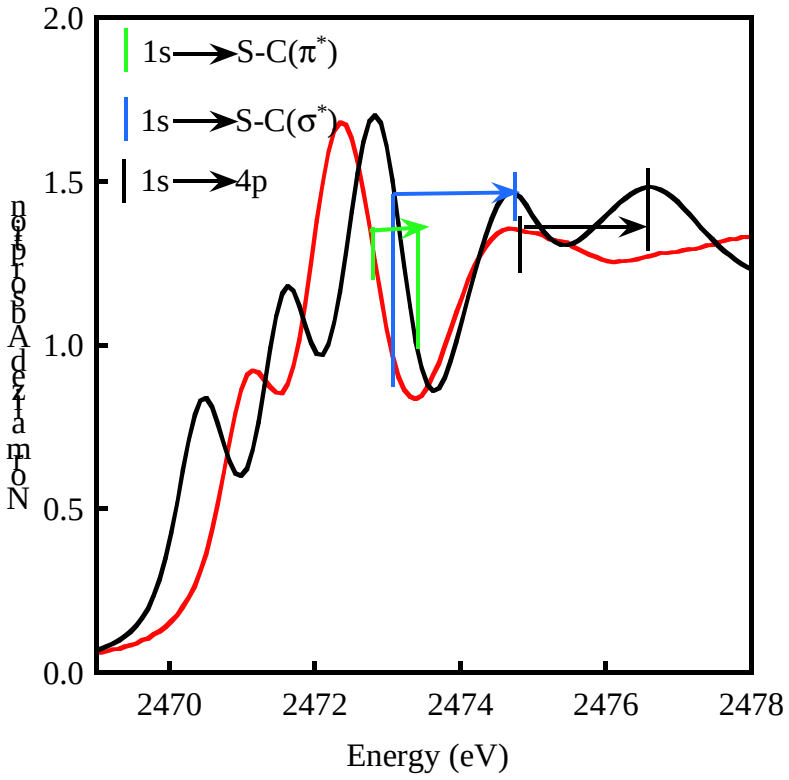

Figure S15. A comparison of the S K-edge XAS spectra of $[MNT]^{2-}$ (—) and **1** (—).The shift in the 1s→S-C(π)*, 1s→S-C(σ)* and 1s→S(4p) transitions upon Cu binding to the free ligand have been depicted by arrows.

The xyz coordinates of the geometry optimized structures of **1**, **1ox**, **2** and **2ox**. Geometry optimizations were performed in Gaussian'03 using BP86 functional with 6-311G* basis set on Cu, Ni and S and 6-31G* basis set on C and N.

1

Cu	0.000000	0.000000	0.000000
S	0.000000	1.649476	1.637064
S	0.000000	-1.649476	1.637064
S	0.000000	-1.649476	-1.637064
S	0.000000	1.649476	-1.637064
N	0.000000	2.053701	5.344455
N	0.000000	-2.053701	5.344455
N	0.000000	-2.053701	-5.344455
N	0.000000	2.053701	-5.344455
C	0.000000	0.698357	3.115803
C	0.000000	-0.698357	3.115803
C	0.000000	-0.698357	-3.115803
C	0.000000	0.698357	-3.115803
C	0.000000	1.423878	4.342227
C	0.000000	-1.423878	4.342227
C	0.000000	-1.423878	-4.342227
C	0.000000	1.423878	-4.342227

1ox

Cu	0.000000	0.000000	0.000000
S	0.000000	1.603228	1.532328
S	0.000000	-1.603228	1.532328
S	0.000000	-1.603228	-1.532328
S	0.000000	1.603228	-1.532328
N	0.000000	2.121790	5.218166
N	0.000000	-2.121790	5.218166
N	0.000000	-2.121790	-5.218166
N	0.000000	2.121790	-5.218166
C	0.000000	0.690211	3.044270
C	0.000000	-0.690211	3.044270
C	0.000000	-0.690211	-3.044270
C	0.000000	0.690211	-3.044270
C	0.000000	1.458249	4.241719
C	0.000000	-1.458249	4.241719
C	0.000000	-1.458249	-4.241719
C	0.000000	1.458249	-4.241719

2

Ni	0.000000	0.000000	0.000000
S	0.000000	1.581443	1.521961
S	0.000000	-1.581443	1.521961
S	0.000000	-1.581443	-1.521961
S	0.000000	1.581443	-1.521961
N	0.000000	2.109458	5.236368
N	0.000000	-2.109458	5.236368
N	0.000000	-2.109458	-5.236368
N	0.000000	2.109458	-5.236368
C	0.000000	0.696903	3.048231
C	0.000000	-0.696903	3.048231
C	0.000000	-0.696903	-3.048231
C	0.000000	0.696903	-3.048231
C	0.000000	1.452883	4.250717
C	0.000000	-1.452883	4.250717
C	0.000000	-1.452883	-4.250717
C	0.000000	1.452883	-4.250717

2ox

Ni	0.000000	0.000000	0.000000
S	0.000000	1.570151	1.491485
S	0.000000	-1.570151	1.491485
S	0.000000	-1.570151	-1.491485
S	0.000000	1.570151	-1.491485
N	0.000000	2.113376	5.190975
N	0.000000	-2.113376	5.190975
N	0.000000	-2.113376	-5.190975
N	0.000000	2.113376	-5.190975
C	0.000000	0.697421	3.005883
C	0.000000	-0.697421	3.005883
C	0.000000	-0.697421	-3.005883
C	0.000000	0.697421	-3.005883
C	0.000000	1.460099	4.207953
C	0.000000	-1.460099	4.207953
C	0.000000	-1.460099	-4.207953
C	0.000000	1.460099	-4.207953

S1. Mulliken population analysis using B3LYP functional.[a]

Complex	Cu	S	C,N
1	45%	48%	7%
1ox	25.5%	66%	8.5%
2	51%	38%	12%
2ox[b]	31%	53%	6%
	45%	44%	5%

.G*on Cu, Ni and S, 6-31G* on C and N. [b]The top and bottom row repr
ψ^*_{SOMO} and $\psi^*_{\beta-LUMO}$ orbitals, respectively.

S2. Comparison of S character in the $\psi^*_{\beta-LUMO}$ and ψ^*_{SOMO} orbitals using previously reporte
oscopically derived I_s with DFT results[a].

Complex	Energy (eV)[b]	Old I_s[b]	New I_s	MPA[a]
$(NEt_4)_2[Ni(S_2C_2Me_2)_2]$	2471.2	82%	62%	53%
$(NEt_4)[Ni(S_2C_2Me_2)_2]$ [b]	2470	74%	59%	60%
	2471	73%	58%	58%
$[Ni(S_2C_2Me_2)_2]$[c]	2470.1	67%	56%	62%
	2471.1	61%	51%	59%

S K-edge data for $[Ni(S_2C_2Me_2)_2]^{0,-1,-2}$ were refit using the same protocol used to fit [Ni(MN
comparison purposes. [b]Pre-edge energies and Mulliken population analysis Reference 25 (r
[c]The top and bottom row represent the ψ^*_{SOMO} and $\psi^*_{\beta-LUMO}$ orbitals, respectively.

Complete references

Reference 36

Frisch, M. J.; Trucks, G. W.; Schlegel, H. B.; Scuseria, G. E.; Robb, M. A.; Cheeseman, J. R.; Montgomery, J., J. A.; Vreven, T.; Kudin, K. N.; Burant, J. C.; Millam, J. M.; Iyengar, S. S.; Tomasi, J.; Barone, V.; Mennucci, B.; Cossi, M.; Scalmani, G.; Rega, N.; Petersson, G. A.; Nakatsuji, H.; Hada, M.; Ehara, M.; Toyota, K.; Fukuda, R.; Hasegawa, J.; Ishida, M.; Nakajima, T.; Honda, Y.; Kitao, O.; Nakai, H.; Klene, M.; Li, X.; Knox, J. E.; Hratchian, H. P.; Cross, J. B.; Bakken, V.; Adamo, C.; Jaramillo, J.; Gomperts, R.; Stratmann, R. E.; Yazyev, O.; Austin, A. J.; Cammi, R.; Pomelli, C.; Ochterski, J. W.; Ayala, P. Y.; Morokuma, K.; Voth, G. A.; Salvador, P.; Dannenberg, J. J.; Zakrzewski, V. G.; Dapprich, S.; Daniels, A. D.; Strain, M. C.; Farkas, O.; Malick, D. K.; Rabuck, A. D.; Raghavachari, K.; Foresman, J. B.; Ortiz, J. V.; Cui, Q.; Baboul, A. G.; Clifford, S.; Cioslowski, J.; Stefanov, B. B.; Liu, G.; Liashenko, A.; Piskorz, P.; Komaromi, I.; Martin, R. L.; Fox, D. J.; Keith, T.; Al-Laham, M. A.; Peng, C. Y.; Nanayakkara, A.; Challacombe, M.; Gill, P. M. W.; Johnson, B.; Chen, W.; Wong, M. W.; Gonzalez, C.; Pople, J. A. "Gaussian 03, revision C.02," 2004